SANDIA REPORT

SAND2010-7085
Unlimited Release
Printed September 2010

Nanopatterned Ferroelectrics for Ultrahigh Density Rad-Hard Nonvolatile Memories

Geoff L. Brennecka, Bruce A. Tuttle, Jeff Stevens, Aaron Gin, David Scrymgeour

Prepared by
Sandia National Laboratories
Albuquerque, New Mexico 87185 and Livermore, California 94550

Sandia National Laboratories is a multi-program laboratory managed and operated by Sandia Corporation, a wholly owned subsidiary of Lockheed Martin Corporation, for the U.S. Department of Energy's National Nuclear Security Administration under contract DE-AC04-94AL85000.

Approved for public release; further dissemination unlimited.

Sandia National Laboratories

Issued by Sandia National Laboratories, operated for the United States Department of Energy by Sandia Corporation.

NOTICE: This report was prepared as an account of work sponsored by an agency of the United States Government. Neither the United States Government, nor any agency thereof, nor any of their employees, nor any of their contractors, subcontractors, or their employees, make any warranty, express or implied, or assume any legal liability or responsibility for the accuracy, completeness, or usefulness of any information, apparatus, product, or process disclosed, or represent that its use would not infringe privately owned rights. Reference herein to any specific commercial product, process, or service by trade name, trademark, manufacturer, or otherwise, does not necessarily constitute or imply its endorsement, recommendation, or favoring by the United States Government, any agency thereof, or any of their contractors or subcontractors. The views and opinions expressed herein do not necessarily state or reflect those of the United States Government, any agency thereof, or any of their contractors.

Printed in the United States of America. This report has been reproduced directly from the best available copy.

Available to DOE and DOE contractors from
U.S. Department of Energy
Office of Scientific and Technical Information
P.O. Box 62
Oak Ridge, TN 37831

Telephone: (865) 576-8401
Facsimile: (865) 576-5728
E-Mail: reports@adonis.osti.gov
Online ordering: http://www.osti.gov/bridge

Available to the public from
U.S. Department of Commerce
National Technical Information Service
5285 Port Royal Rd
Springfield, VA 22161

Telephone: (800) 553-6847
Facsimile: (703) 605-6900
E-Mail: orders@ntis.fedworld.gov
Online ordering: http://www.ntis.gov/help/ordermethods.asp?loc=7-4-0#online

SAND2010-7085
Unlimited Release
Printed September 2010

Nanopatterned Ferroelectrics for Ultrahigh Density Rad-Hard Nonvolatile Memories

Geoff L. Brennecka and Bruce A. Tuttle
Electronic and Nanostructured Materials Department

Jeff Stevens
MESAFab Engineering Department

Aaron Gin and David Scrymgeour
Photonic Microsystems Technology Department

Sandia National Laboratories
P.O. Box 5800
Albuquerque, NM 87185-1411
contact: glbrenn@sandia.gov

Abstract

Radiation hard nonvolatile random access memory (NVRAM) is a crucial component for DOE and DOD surveillance and defense applications. NVRAMs based upon ferroelectric materials (also known as FERAMs) are proven to work in radiation-rich environments and inherently require less power than many other NVRAM technologies. However, fabrication and integration challenges have led to state-of-the-art FERAMs still being fabricated using a 130nm process while competing phase-change memory (PRAM) has been demonstrated with a 20nm process. [1] Use of block copolymer lithography is a promising approach to patterning at the sub-32nm scale [2], but is currently limited to self-assembly directly on Si or SiO_2 layers. Successful integration of

ferroelectrics with discrete and addressable features of ∼15-20nm would represent a 100-fold improvement in areal memory density and would enable more highly integrated electronic devices required for systems advances. Towards this end, we have developed a technique that allows us to carry out block copolymer self-assembly directly on a huge variety of different materials and have investigated the fabrication, integration, and characterization of electroceramic materials–primarily focused on solution-derived ferroelectrics–with discrete features of ∼20nm and below. Significant challenges remain before such techniques will be capable of fabricating fully integrated NVRAM devices, but the tools developed for this effort are already finding broader use. This report introduces the nanopatterned NVRAM device concept as a mechanism for motivating the subsequent studies, but the bulk of the document will focus on the platform and technology development.

Acknowledgment

The authors would like to extend their gratitude to Jon Ihlefeld, Kelsey Meyer, Chris Shelton, Chad Parish, and Bonnie McKenzie of Sandia National Laboratories; Prof. Bill Fahrenholtz and Harlan Brown-Shaklee of Missouri S&T; Prof. Jacob Jones and Krishna Nittala of the University of Florida; Prof. Paul Nealey, Shengxiang Ji, and Prof. Padma Gopalan of the University of Wisconsin; Prof. John Ekerdt, Ryan Fitzpatrick, and Wyatt Winkenwerder of the University of Texas at Austin; and Alp Sehirlioglu of NASA Glenn Research Center and Case Western Reserve University for their valuable discussions and technical assistance throughout the duration of this project.

Contents

Summary **11**

Nomenclature **12**

1 Introduction **15**

2 Patterning **19**

3 Integration **25**

4 Analysis **29**

5 Conclusions **33**

References **34**

List of Figures

1.1 Schematic of BCP thin film mask 17

2.1 PS mask oriented on Si 20

2.2 PS mask oriented on MgO 20

2.3 PS mask oriented on ZnO 20

2.4 PS mask oriented on PZT 20

2.5 PS mask oriented on ZrB_2 20

2.6 PS mask oriented on Pt 20

2.7 Graphoepitaxy schematic 21

2.8 Successful graphoepitaxy 21

2.9 Chemical patterning schematic 22

2.10 Patterned solution-derived PZT 23

2.11 Large-area solution-patterned TiO_2 23

2.12 Patterned solution-derived TiO_2 23

2.13 Patterned sputtered Ti 23

2.14 Schematic of MgO-mediated PZT patterning 24

2.15 e-beam defined patterned PZT 24

2.16 Patterned Pt/PZT on Pt//Si substrate 24

3.1 Ostwald ripening of discrete nanofeatures 25

3.2 MgO-coated PZT nanofeatures after crystallization 26

3.3 MgO etch mask trials 27

4.1 *in-situ* X-ray diffraction of PZT-based film crystallization 29

4.2 Spectral Imaging 30
4.3 Quantitative chemical mapping via spectral imaging 31
4.4 Schematic illustration of a PFM setup 31
4.5 PFM data from micropatterned PZT films 32
4.6 AFM scan of nanopatterned amorphous PZT features 32

List of Tables

1.1 NVRAM characteristics 16

Summary

This project investigated patterning and integration techniques that would be compatible with PZT-based ultra-high density rad-hard NVRAM. In particular, the project focused on extending lithography techniques based on the directed self assembly of block copolymers to non-Si/SiO_2 substrate layers and studied techniques for integrating these discrete and ordered $\sim$20nm features into functional device structures. In addition to developing a fabrication platform that enables the formation of nanoscale feature of essentially any material that can be deposited by sputtering and/or chemical solution into ordered nanofeatures, this project also initiated in-depth *in-situ* diffraction studies of PZT-based thin films, laid the groundwork for etching and pattern transfer from and into a variety of non-standard materials at the extreme nanoscale, and developed characterization and analysis tools that can determine quantitative chemical distribution at the $\leq$5nm scale.

Nomenclature

FERAM Ferroelectric Random Access Memory

NVRAM Non-Volatile Random Access Memory

IC Integrated Circuit

PZT $Pb(Zr,Ti)O_3$, a family of ferroelectric and piezoelectric ceramic materials

RF MEMS Radio Frequency MicroElectroMechanical Systems

PRAM RAM built around the change in resistance that accompanies a phase change, typically between amorphous and crystalline forms of chalcogenide materials

SONOS Silicon-Oxide-Nitride-Oxide-Silicon RAM similar in function to flash but using Si_3N_4 instead of polysilicon for the charge storage layer

CNT-RAM RAM based on hysteretic mechanical deflection of carbon nanotubes (CNT).

RRAM RAM based on a change in resistivity of transition-metal-containing layers as a function of processing and electrical pulse history

BCP Block copolymer, two or more immiscible polymers covalently bound together

ITRS International Technology Roadmap for Semiconductors

PS polystyrene

PMMA poly(methylmethacrylate)

DSA Directed Self Assembly

LER Line Edge Roughness, a measure of the uniformity of lithographically-defined lines and features

NMP N-methyl-2-pyrrolidone, a solvent

SEM Scanning Electron Microscope

Pt//Si Si substrate coated with Pt and adhesion layers; here refers to Si coated with 400nm thermal SiO_2, 40nm TiO_x and 170nm Pt

TEM Transmission Electron Microscopy

EDS Energy Dispersive Spectroscopy

SI Spectral Imaging, a technique for collecting, in this case, full x-ray spectra as a beam is rastered across a sample followed by post-collection data analysis

PCA Principal Component analysis, a statistical method for deconvolution of signals from a finite number of discrete overlapping sources

MVSA Multi-Variate Statistical Analysis, a matrix-based statistical method for analysis of a (relatively) large number of co-varying but not necessarily dependent values

AFM, PFM Atomic Force Microscopy and Piezoresponse Force Microscopy, respectively; cantilever deflection-based techniques for measuring topography and/or electromechanical response of materials with nanometer-scale resolution

Chapter 1

Introduction

Ferroelectric random access memory (FERAM) possesses several attractive characteristics when compared to other types of non-volatile memory (NVRAM) technologies (see Table 1.1), especially for low-power operation in challenging environments, but it is currently fabricated at areal bit densities 10-100x lower than competing technologies. Defining <30nm features is a challenge for the entire integrated circuit (IC) community, but three additional and significant hurdles stand in the way of using present technology to scale FERAM fabrication to the nanoscale: integration, crystallinity, and potential lateral size effects. The most common and best-performing ferroelectric materials for FERAM are those in the $Pb(Zr,Ti)O_3$ family (collectively referred to here as 'PZT') but the propensity for severe reaction between Pb and Si requires the use of buffer layers and, commonly, metallic electrodes between any Si-containing layers and PZT. Ferroelectricity is a collective phenomenon that emerges from the interactions of neighboring unit cells of a polar (*i.e.* possessing a spontaneous polarization) crystalline material. Since PZT layers are typically deposited from chemical solution or via one of several vapor phase techniques, they require thermal annealing to crystallize, typically at temperatures $\geq$650°C. This thermal treatment step is associated not only with the phase transition(s) involved in crystallizing the PZT layer, but also some poorly-understood interactions between the PZT layer and the underlying electrode material (often Pt).

Under all but the most precisely controlled conditions, the PZT layer will crystallize into a complex polycrystalline layer. Depending upon stoichiometry and processing conditions, this resulting crystalline layer may or may not exhibit a preferred crystallographic orientation with individual crystallite grains ranging in size from a few nanometers to a micron or more. Grains of different orientations exhibit significantly different ferroelectric behavior, and the boundaries between such grains lead to additional complexity, both in terms of electrical response and the chemical reactivity that is critical for etch behavior. Presently, integrated ferroelectric films, whether for use in FERAM, RF MEMS, or other applications, are patterned by depositing blanket films and then etching away everything except for the desired functional regions.[3] Besides severely degrading the electrical properties of ferroelectric materials at and near either wet or dry chemical etch boundaries, [4, 5, 6] this etch process represents a serious limitation to the down-scaling of FERAM fabrication technology because of the difficulty in achieving reasonable etch anisotropy in such systems. In addition, the emergent nature of the ferroelectric response means that there must be some fundamental minimum size below which electric field-driven reversal of the spontaneous polarization will be impossible, thereby setting an absolute minimum feature size for ferroelectric memory elements. Recent experiments have shown that the ferroelectric response can persist

Table 1.1. Reported characteristics for NVRAM technologies.

Type	Pixel Size	Rad-Hard?	Oper. Voltage	Reset Power	Minimum Current	Fatigue Resistance	Data Retention	Read/ Write	Temperature Stability	Notes
Magnetic (spin devices)	∼100nm device; ∼50nm pixel; ∼10nm thick	Yes			1-10mA	Claimed unlimited	Inversely proportional to required write current	5-100ns	scales with write current; limited by Nèel temperature	1T1C required today; potentially crossbar and racetrack compatible
PRAM (phase change, resistive)	∼20nm diameter, ∼3nm thick	Yes	0.5 - 1V	10-100μW per pixel	0.25mA	10^{13} cycles	>10yrs at 130°C	1ns – 100ms	very stable up to >100°C	BAE using Ovonyx; limited by ΔH_f of ∼600J/cm^3
SONOS	∼20-40nm	Yes	∼2-4.5V			10^8 cycles		>100ns	Stability decreases with voltage and size	Very similar to flash memory
CNT-RAM	∼100nm across, ∼15nm thick	Possible	1-5V		0.01mA	Claimed unlimited	Claimed unlimited	<100ns	Unknown; probably poor at elevated temps	Arrayed crossbar compatible
FERAM	∼130nm now, ∼20nm feasible	Yes	1.5V now; <1V feasible		0.1 mA	$>10^{16}$	>10yrs at 85^{circ}C	<100ns	Retention suffers above ∼100°C	Commercially available at 1T1C; crossbar compatible
RRAM (resistance changes)	10s of nm; limited by connec-tion to circuit	Doubtful	Values all over the board; this technology is still very young. While it shows promise (largely because of the simplicity of manufacture and multi-state capabilities), the science behind its operation (essentially defect/charge trapping at interfaces) is still being investigated.					1ns - 100ms	Unknown; retention will likely suffer above ∼50-100°C	Multi-state possible; crossbar compatible

for continuous epitaxial films as thin (in the direction of the applied electric field) as 3 unit cells (∼1.2nm), [7, 8] but there has not yet been a systematic study of the effect(s) of lateral feature size on the existence and magnitude of ferroelectric polarization reversal. In order to address these fabrication scaling limitations and–ideally–provide a platform for performing systematic studies of feature size scaling effects on the ferroelectric response, we undertook the development of a technique that would be capable of fabricating discrete and addressable nanoscale features of ferroelectric PZT.

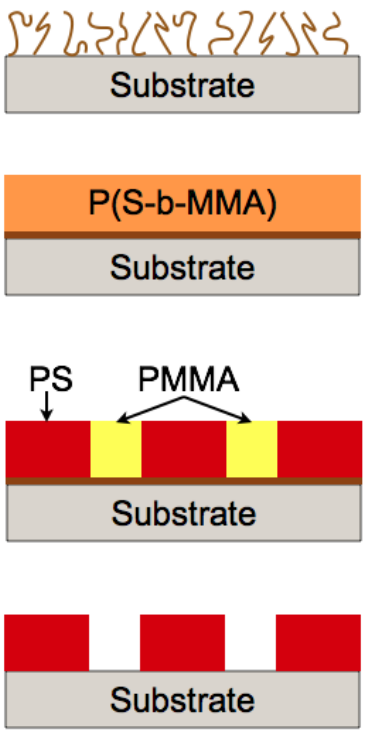

Figure 1.1. Schematic of BCP thin film mask

Block copolymers (BCP) consist of two chemically different polymer blocks that are driven to phase separate by their chemical incompatibility but are constrained by the fact that the blocks are covalently bound to one another. The resulting microphase separation can produce ordered equilibrium morphologies such as ordered arrays of spheres, bicontinuous spinodal (gyroid) morphologies, or lamella. [9, 10, 11, 12] The small dimensions (commonly ∼10-50nm) associated with these structures makes them interesting for a variety of applications, and their promise for lithography in particular has attracted a great deal of interest over the past dozen years. [13, 14, 15, 16] In practice, surface interactions with the substrate complicate equilibrium, introducing significant challenges for researchers but also providing an opportunity for additional control over achievable morphologies. [17] Research on block copolymer lithography has progressed to the point where it has been included on the ITRS roadmap as a potentially-feasible solution for patterning at and below the 22nm node. [2] A very simple schematic representation of this concept is shown in Figure 1.1. A thin surface layer is used to neutralize the substrate surface to prevent either block of the subsequently-deposited copolymer thin film (illustrated here as PS-b-PMMA) from preferentially wetting the surface. During annealing, these blocks separate to form, for example, lines or cylinders. Removal of the PMMA block leaves a PS mask with nanoscale openings.

The overall goal of this project was to examine promising avenues for the eventual fabrication of integrated nanoscale ferroelectric structures with a particular focus on identifying and investigating patterning, processing, and performance challenges. Aspects that received the greatest attention were:

- Extension of BCP-based lithography to a variety of substrate materials compatible with the patterning of ferroelectric nanofeatures
- Expansion of pattern transfer capabilities to accommodate the integration of these non-standard material in an integrated process
- Combining BCP-based pattern definition techniques with solution-based fabrication routes
- Optimizing the fabrication of PZT-based ferroelectrics from chemical solution through advanced characterization and analysis

Chapter 2

Patterning

In order for BCP lithography to be useful for the pattern definition of Si-incompatible materials such as PZT, it is important that the BCP can be assembled on materials other than Si/SiO_2. In theory, this simply involves neutralizing the surface of the desired substrate such that neither block preferentially adheres to the surface; in practice, this requires the development of a brush layer that can be grafted to essentially any surface, yet still present a neutral surface to an overlying BCP layer. Our collaborators at the University of Wisconsin, Profs. Padma Gopalan and Paul Nealey as well as their graduate students, were able do just this, as described in more detail elsewhere [18]. This custom-engineered polymer brush layer enables the assembly of vertically-oriented PS-b-PMMA cylinder-forming diblock copolymers on essentially any substrate including, for example, Si with native oxide (Figure 2.1), MgO (Figure 2.2), ZnO (Figure 2.3), PZT (Figure 2.4), and even ZrB_2 (Figure 2.5). Attempts to graft the brush layer directly to Pt did meet with difficulty, though when the Pt layers were coated with as little as 3nm of Ti that then formed a native oxide layer, grafting the neutral brush and subsequent BCP assembly were successful (Figure 2.6).

Once features of the proper size can be produced, they must be patterned in a controlled manner such that they could be arbitrarily addressed. As evident from Figures 2.1 – 2.6, the basic self assembly process that defines the mask via phase separation produces features that are relatively uniform in size and shape and that exhibit reasonable short-range order but which are entirely disordered beyond the first few nearest neighbors, severely limiting their utility for electronic devices which require that each pixel feature be individually addressable. By introducing additional constraints to the system, the self assembly process can actually be directed to impart long-range order on the resulting pattern. One such directed self assembly (DSA) approach uses an initial photolithography and shallow anisotropic etch procedure to introduce guides to the substrate which geometrically confine assembling features, as illustrated schematically in Figure 2.7. This technique, generally referred to as 'graphoepitaxy,' has been successfully demonstrated with line- and cylinder-forming BCP masks across multiple micron length scales, and the use of regularly-spaced posts within an otherwise empty field has been shown to successfully maintain order over relatively large areas as well [19, 20, 21]. Working with our collaborators at the University of Texas-Austin (Prof. John Eckerdt and his students), we too have successfully demonstrated graphoepitaxy of PS-b-PMMA BCP (see Figure 2.8). DSA can also effectively shrink the relevant feature pitch by integral multiples. In other words, using Figure 2.8 to illustrate, the initial photolithographically-defined feature is 210nm wide, but the resulting ordered BCP features are only 21nm in diameter, essentially resulting in a 10-fold reduction in feature pitch–or, expressed another way, 10x density multiplication.

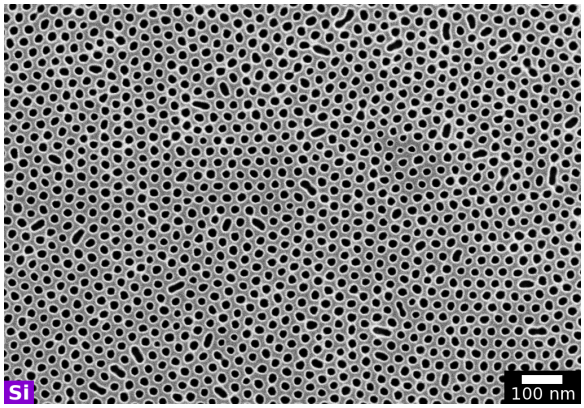

Figure 2.1. PS mask oriented on Si

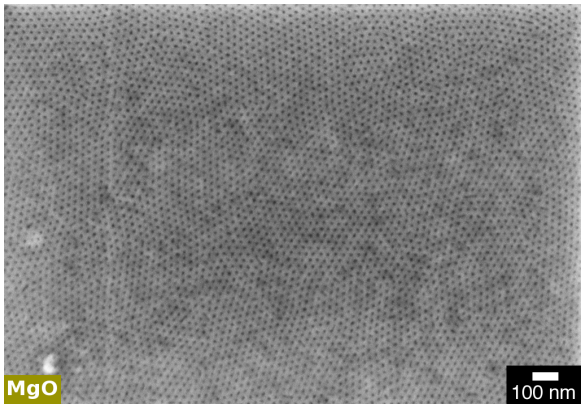

Figure 2.2. PS mask oriented on MgO

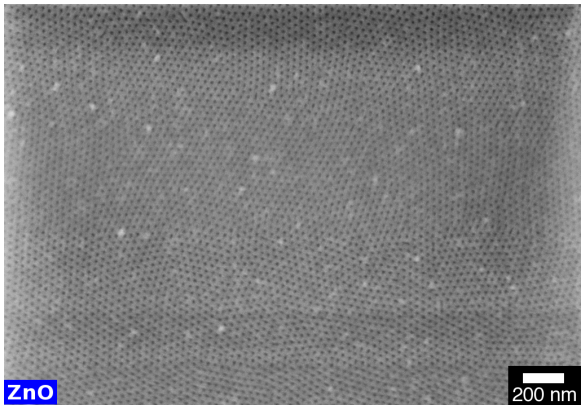

Figure 2.3. PS mask oriented on ZnO

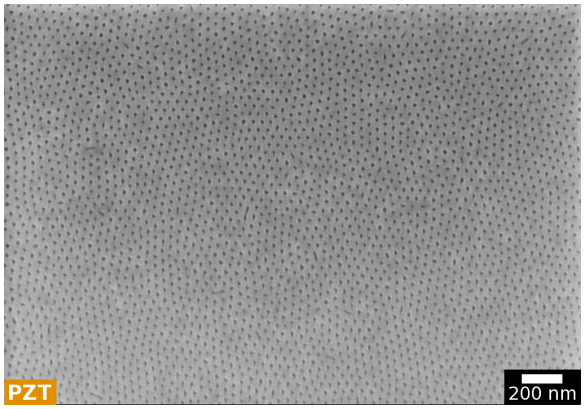

Figure 2.4. PS mask oriented on PZT

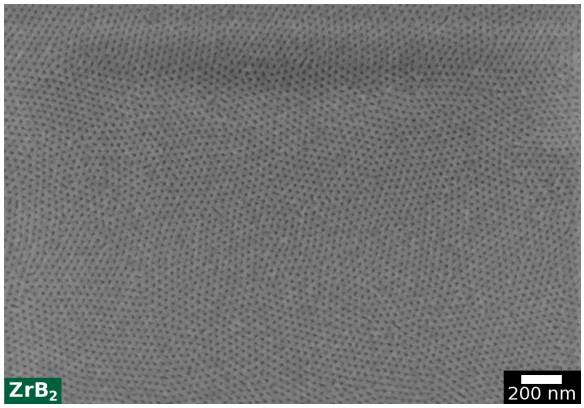

Figure 2.5. PS mask oriented on ZrB_2

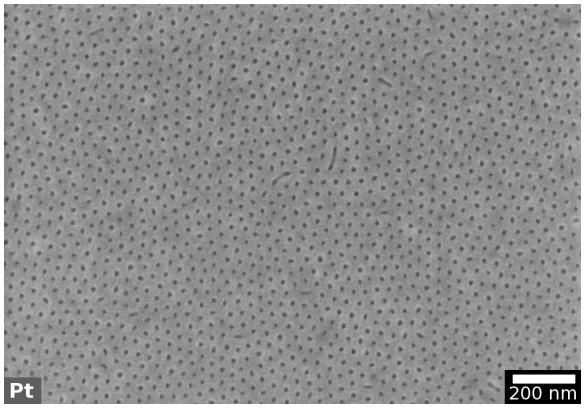

Figure 2.6. PS mask oriented on Pt

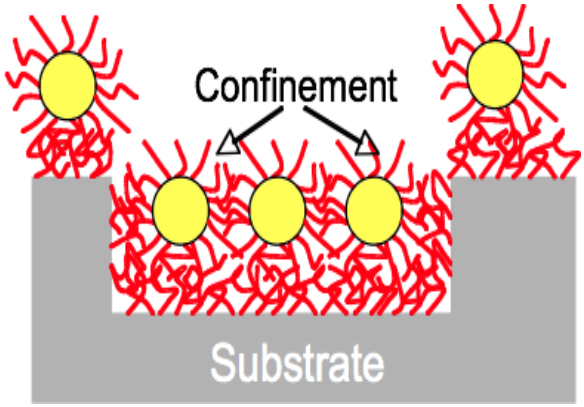

Figure 2.7. Graphoepitaxy schematic (adopted from [20])

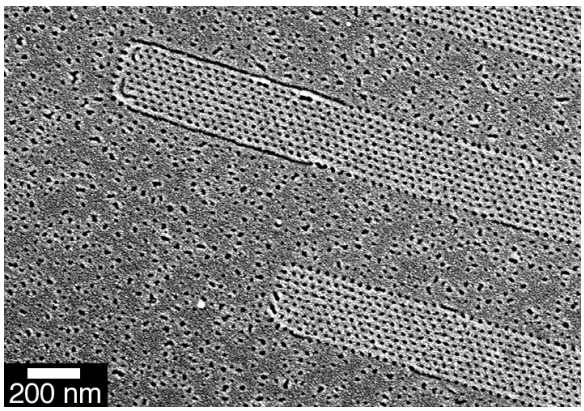

Figure 2.8. Successful graphoepitaxy

While graphoepitaxy is an effective approach to extending long-range order, its drawbacks include difficulty in controlling exactly where individual features will be located (note, for example, the 'outline' of the geometric confinement seen in Figure 2.8) and the disruption of the planarity of the substrate layer which could be problematic for some processes. Prof. Paul Nealey's group at the University of Wisconsin, with whom we also collaborated on this project, have pioneered an alternative approach to DSA that is based on the use of a photo-patternable brush layer which allows one to control the relative preference of each copolymer block to wet the substrate. This chemical patterning approach provides fine control over the very thermodynamic interactions that lead to the copolymer phase separation in the first place, with resolutions of standard photolithography and without the requirement of any etch procedures. This process is illustrated schematically in Figure 2.9.

One large advantage of chemical patterning over graphoepitaxy is the fact that the thermodynamic wetting-based control of the substrate-mask interactions and the finite polymer block lengths actually combine to improve the line edge roughness (LER) of patterned features [22, 23]. In addition, the geometric constraints of the initial pattern are less stringent than for graphoepitaxy. For example, successful graphoepitaxy requires that the spacing between the confining walls and the associated neutralizing brush layer be an exact multiple of the block pitch for successful pattern assembly, but chemically-patterned substrates can actually produce high-quality well-ordered BCP patterns even when the underlying chemical pattern varies by as much as $\pm 10\%$ from the polymer block pitch.

This combination of finer control of the associated driving forces and relaxed constraints on the initial 'directing' pattern means that the BCP mask layers whose assembly is directed by a chemically-patterned substrate can actually be of higher quality than the initial directing pattern in terms of feature regularity and general pattern fidelity, even when combined with density multiplication [23]. In addition, the fact that the directing pattern is now in the brush layer that sits on top of the substrate rather than etched into the substrate layer itself means that the substrate remains planar. This also allows the directing pattern to be extended across very large areas, extending the BCP order from a handful of nearest neighbors to mm^2-scale or larger areas.

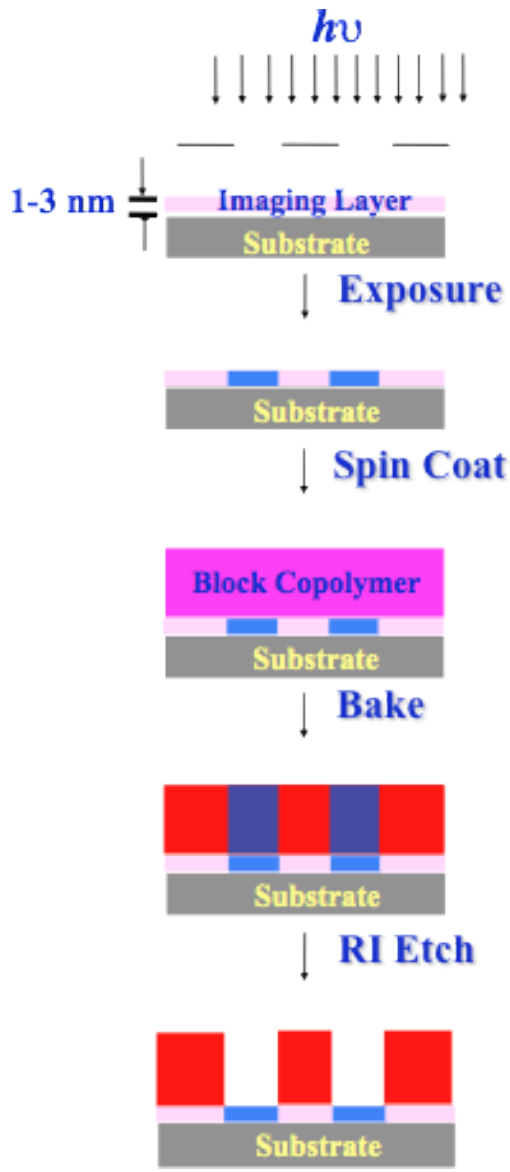

Figure 2.9. Schematic illustration of chemical patterning using the photopatternable brush layer developed at UW [24].

One of the goals of this project was to develop a fabrication technique that resulted in nanoscale ferroelectric features without actually chemically etching the ferroelectric material itself. Since the solution- and vacuum-based deposition techniques that lead to ferroelectric thin films with the best properties are blanket deposition approaches, a lift-off step is an attractive alternative to chemical etching. The polystyrene masks are ideal for this since they are robust enough to survive the initial deposition steps (whether in vacuum for sputter deposition, for example, or the spin coating and drying steps associated with solution deposition) but are easily removed by solvents such as NMP (N-methyl-2-pyrrolidone) or toluene that do not affect the patterned materials of most interest (metals and metal-oxides). Figures 2.12 and 2.13 demonstrate the effectiveness of this approach.

To fabricate these discrete nanopillars, the UW-developed neutral brush layer was first grafted to the substrate of interest (here, MgO-coated Pt//Si wafers). The PS-b-PMMA BCP layer was then assembled on top of this neutral brush and the vertical orientation of the PMMA columns was verified by SEM. A brief UV exposure followed by a ∼10sec rinse in acetic acid removed the PMMA blocks, leaving a ∼32nm thick PS layer with ordered, vertically-arranged holes. A descum step (a low-power oxygen plasma etch is the preferred route) removes the neutral brush layer that remains at the bottom of these 'holes' in the mask, exposing the MgO layer. At this point, the 'filler' material is deposited. For sputter-deposited features (see for example, Figure 2.13), a thin layer of material is sputtered across the entire sample. Since for the particular BCP composition used here the PS layer is only ∼32nm thick and the 'holes' are ∼32nm thick, one must be careful not to sputter a layer that is thick enough to become continuous or the subsequent liftoff step will be problematic. Similarly, for successful liftoff, solution-deposited layers also need to become discontinuous in order to allow solvent infiltration and PS removal. This is easily accomplished by using a low-concentration solution. Figure 2.12 shows features that were deposited from an initial 0.025M solution of $Ti(OiPr)_4$ using acetic acid as a chelating agent and methanol as a solvent. This solution was dispensed onto the sample and allowed to sit for ∼5sec before spinning at 4000rpm to planarize and remove excess solution. The sample was then dried at 100°C for 10min to remove excess solvent and gel the precursor sufficiently to avoid its removal with the PS. After cooling to room temperature, the

sample was immersed in NMP and placed in an ultrasonic bath for 5min then removed and rinsed with toluene before returning to 5 additional minutes of ultrasonic NMP treatment followed by a final toluene rinse, leaving discrete nanopillars of amorphous TiO_2 gel.

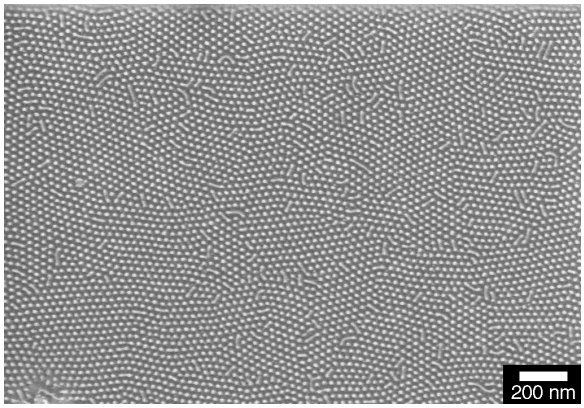

Figure 2.10. Patterned solution-derived PZT

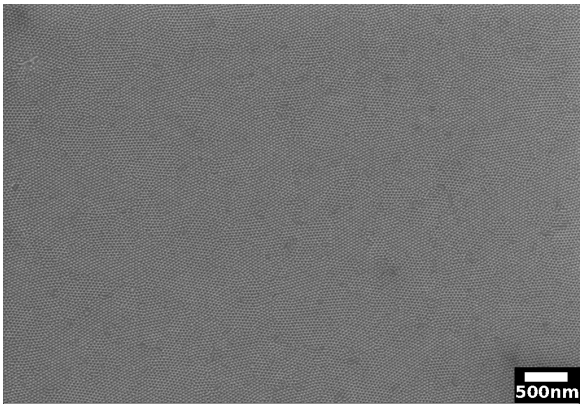

Figure 2.11. Large-area solution-patterned TiO_2

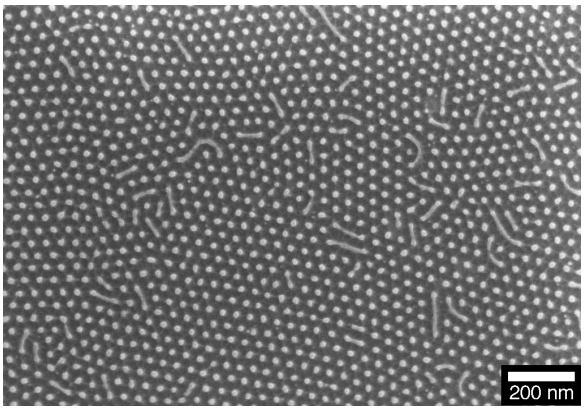

Figure 2.12. Patterned solution-derived TiO_2

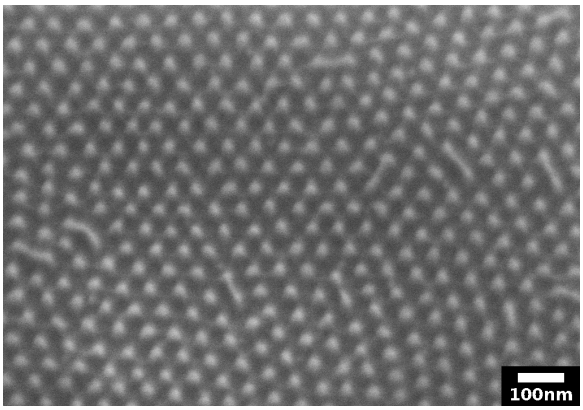

Figure 2.13. Patterned sputtered Ti

One of the great advantages of this approach is that the only limitation to the materials that can be deposited in this fashion is that they have to be compatible with some sort of thin blanket deposition technique, which is not a very limiting condition. For example, the PZT solutions that our group has used for years for successfully fabricating capacitor films [25, 26] are closely related to the simple solution used to deposit the TiO_2 features seen in Figure 2.12, so it should not be surprising that the same process works quite well for fabricating amorphous nanofeatures of PZT directly on Pt//Si substrates (Figure 2.10). Such solutions readily fill the PS mask and appear not to be affected at all by the NMP PS removal process, as illustrated well by the large area shown in Figure 2.11 where the only defects visible are direct reproductions of the defects in the original PS mask layer.

To investigate additional liftoff-based approaches to patterning ferroelectrics, we used e-beam lithography to create complex patterns on top of MgO-coated Pt//Si substrates. After developing the resist, the substrate was soaked in a weak oxalic acid solution (0.005M) for 5min to etch through the exposed regions of the ∼50nm-thick MgO layer and then rinsed with deionized water. After removal of the PMMA-based e-beam resist, a standard PZT solution was spin-deposited across this patterned sample and subjected to our standard PZT processing cycle which includes a 400°C pyrolysis step and 10min at 700°C for crystallization. The sample was again soaked in oxalic acid to remove the remaining MgO and liftoff any overlying PZT. This approach successfully resulted in a patterned layer of ∼35nm-thick PZT (Figure 2.15) as defined by the original e-beam pattern. Further, piezo force microscopy (PFM) measurements (see Chapter 4 for more details about the PFM technique and associated measurements) confirmed that the patterned PZT exhibited a hysteretic piezoelectric response, strongly suggesting that it was ferroelectric even when patterned into the complex shape of a CINT logo. Finally, as further demonstration of the capabilities of this MgO-mediated patterning and liftoff approach, we carried out the same process again, only between the PZT crystallization process and the MgO-removal liftoff step we also sputter deposited a blanket Pt layer to serve as a top electrode (see schematic in Figure 2.14). After successful removal of the MgO and overlying PZT and Pt layers, we were left with a Pt/PZT/Pt capacitor structure having an arbitrary shape defined by e-beam lithography (Figure 2.16).

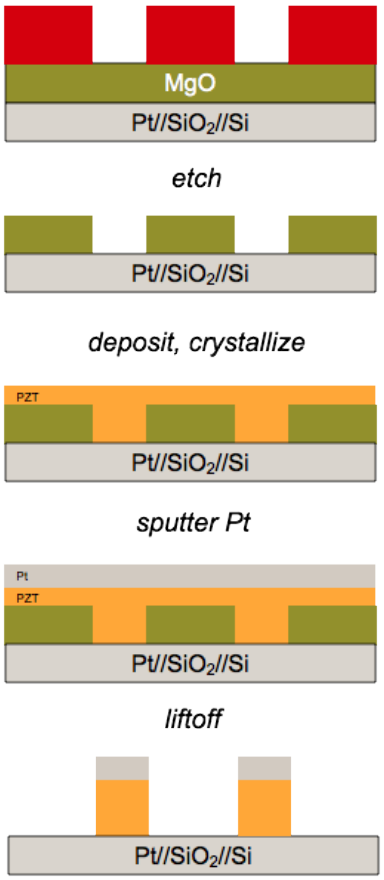

Figure 2.14. Schematic of MgO-mediated PZT patterning

Figure 2.15. e-beam defined patterned PZT

Figure 2.16. Patterned Pt/PZT on Pt//Si substrate

Chapter 3

Integration

Formation of nanoscale features makes for nice images, but to be useful in a device, such features must be functional when integrated into a device-relevant process flow. For the specific case of the PZT nanofeatures of interest here, this requires that the PZT be crystallized without undergoing any deleterious reactions with nearby materials and that the individual pixels be connected to the rest of the electronic device in some way. The most likely strategy for addressing nanoscale FERAM pixels would be to use some variant of the crossbar architecture[27, 28]; the remainder of this chapter will focus on the challenges of integrating PZT-based nanofeatures into a relevant fabrication process.

The features shows in Figures 2.12 – 2.11 are amorphous; in order to exhibit any ferroelectric response, they must be crystalline. Continuous solution-deposited PZT films are crystallized by heating to ∼700°C, but because of Ostwald ripening, simply heating the amorphous nanofeatures will destroy their discrete and ordered nature (Figure 3.1).

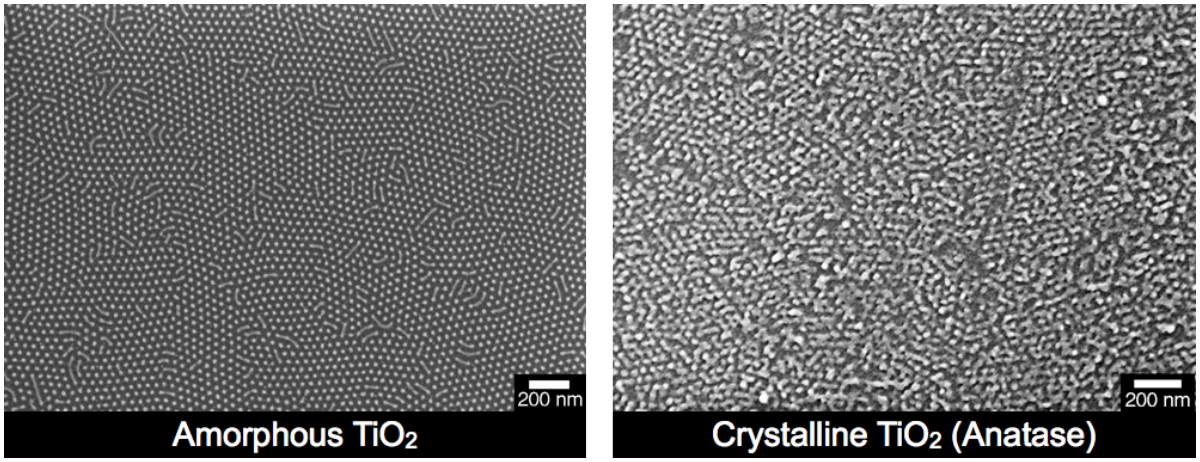

Figure 3.1. Sufficient thermal energy to crystallize discrete nanofeatures (TiO_2 shown here) also results in Ostwald ripening which destroys the BCP-imparted order.

Thus, in order to crystallize freestanding PZT nanofeatures without destroying their order, it is necessary to immobilize them somehow during thermal treatment in a way that does not lead to harmful chemical reactions and, ideally, allows their return to discrete, free-standing features

after crystallization. The list of materials with which PZT is known not to react when in intimate contact at ∼700°C and which are easily removed by some sort of treatment–ideally a simple wet-etch–that does not harm crystalline PZT is extremely short. MgO is a common substrate that has been used for PZT crystalline studies which have shown no evidence of reaction during thermal processing, and–as shown in Chapter 2–can be removed using an oxalic acid wet etch that appears not to damage crystalline PZT.

One conceptually-simple approach is to fabricate the amorphous nanofeatures just as discussed in Chapter 2 and then to coat these samples with a blanket of sputtered MgO before heating the sample to crystallize the PZT, followed by a MgO-removing oxalic acid rinse. Under this approach, the complication of then applying appropriate circuitry to individually address the nanofeatures is not addressed. Figure 3.2 shows the result of such a process: the features are ∼150% their original diameters and appear to have lost some of the original short-range order. Additionally, the rough surfaces and poor dielectric response of these features suggested that some sort of reaction was occurring during thermal processing; chemical analysis of MgO layers sputtered on the same instrument for a different effort indicated significant alkaline contamination which may explain some of the problems seen in the sample shown in Figure 3.2.

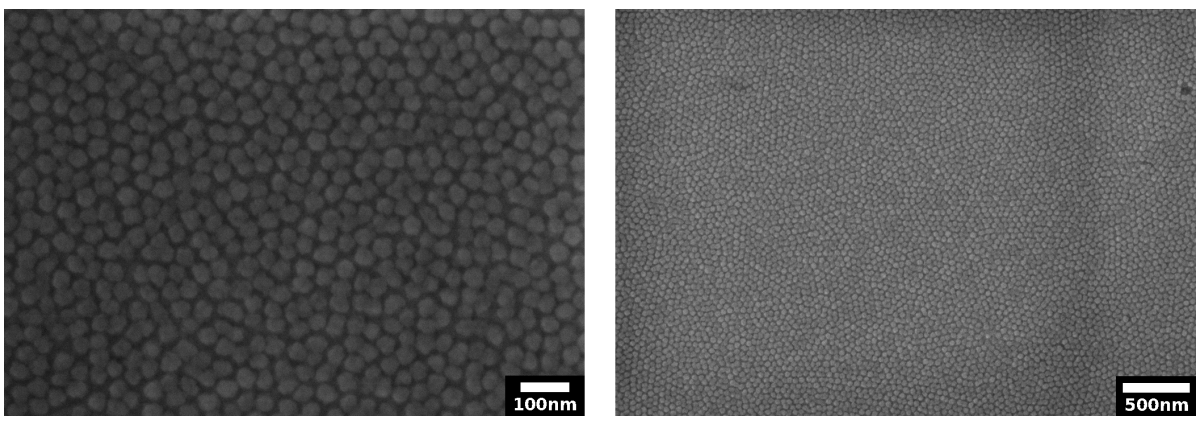

Figure 3.2. MgO was sputter-deposited over amorphous PZT nanopillars similar to those shown in Figure 2.10 followed by a crystallization heat treatment of 700°C for 10min and subsequent oxalic acid MgO removal.

A preferred approach to providing a robust inert matrix for PZT nanofeature crystallization would be to directly transfer the BCP-defined pattern from the PS into the inert layer (MgO, for example) prior to PZT solution deposition. The process flow for such a process would look nearly identical to Figure 2.14 where the initial pattern is defined in this case not by e-beam lithography but instead by BCP lithography. Unfortunately, while wet etching MgO using oxalic acid is straightforward, dry etching MgO is anything but simple. Exhaustive studies led by Jeff Stevens were unable to determine appropriate conditions for dry etching MgO with a PS mask; selectivity values were typically ∼0.1-0.2, which, for PS layer thickness of only ∼32nm was simply insufficient for effective pattern transfer directly into MgO. Continued etch recipe development efforts (see Figure 3.3 for an example of a small subset of such data) eventually resulted in a multi-material stack consisting of PS//SiO_2//Cr//MgO//Pt which, according to individual etch-pair

selectivities studied separately should enable the transfer of a BCP-defined pattern into an MgO layer on Pt//Si. Unfortunately, this development occurred too late in the project to allow in-depth studies of the maintenance of pattern quality during these etch steps, so it is presently unknown whether this stack and the associated etch recipes would allow pattern transfer into MgO for direct PZT infiltration and crystallization.

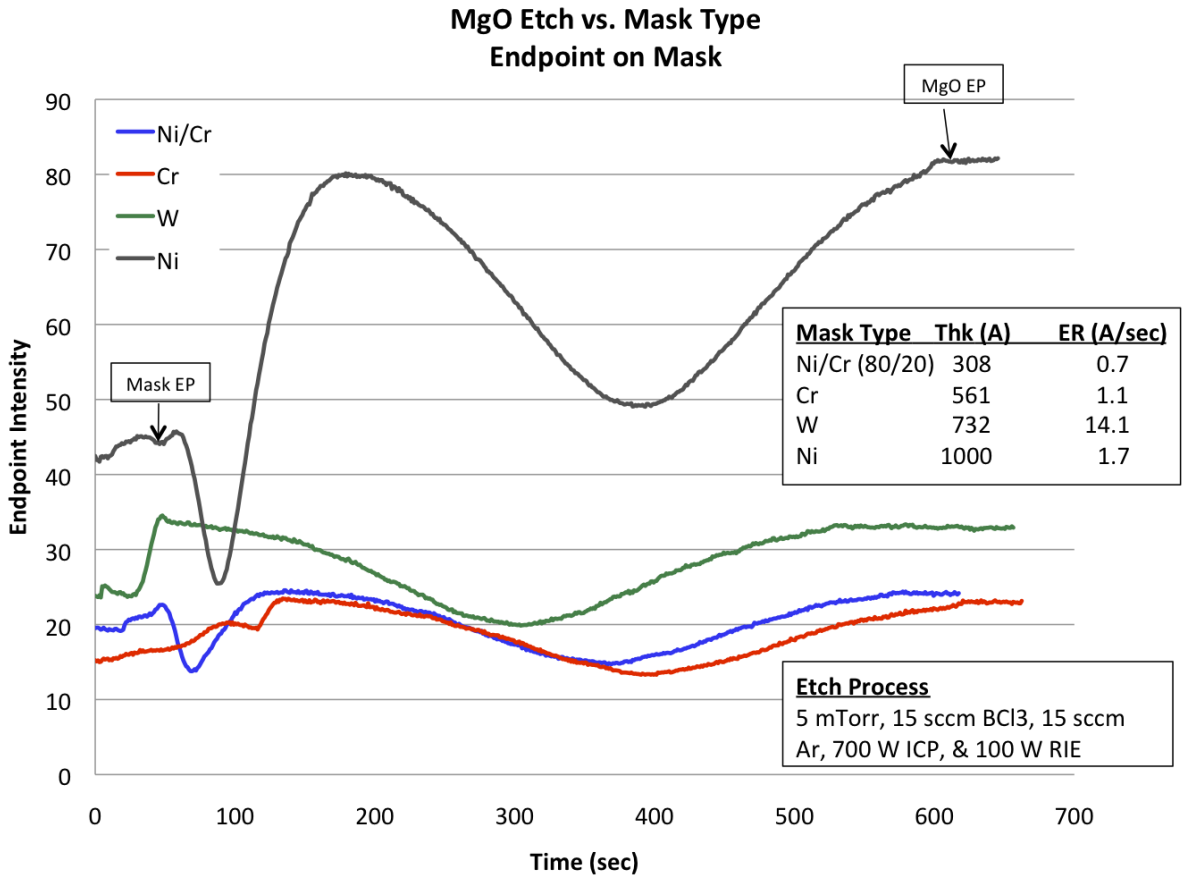

Figure 3.3. A large number of materials and parameters were studied in an attempt to develop a reliable dry etch recipe for MgO and, ideally, a technique for transferring the BCP-defined pattern into an MgO layer. The above plot shows but a very small subset of such data.

The difficulties of maintaining PZT feature fidelity during thermal treatment highlighted the need for better understanding of the phase transformations and other chemical interactions that occur during the crystallization process of solution-derived PZT thin films, particularly on Pt//Si substrates. This led to a project demand for improved thermal processing of PZT thin films, which in turn led to a focus on the development and use of appropriate analytical techniques for evaluating solution-derived nanoscale PZT during and after thermal processing.

Chapter 4

Analysis

It has long been recognized that both the substrate and the thermal profile exert strong influences on the phase and texture evolution of solution-derived PZT thin films during thermal processing, but since all prior studies were carried out *ex-situ*, an understanding of the complex phase and interface reactions was lacking. Through a collaboration with Prof. Jacob Jones and his group at the University of Florida, we initiated an *in-situ* X-ray diffraction-based study of PZT-based thin films on Pt/Si substrates during thermal processing which has since expanded into a major component of a separate project. The initial studies carried out under this project were instrumental in establishing the phase progression (amorphous → interfacial Pt_xPb intermetallic → fluorite → perovskite) as well as showing that the formation of the Pt_xPb phase could be avoided by shunning the common practice of compensating for Pb-species volatility through the use of super-stoichiometric precursor solutions (Figure 4.1).

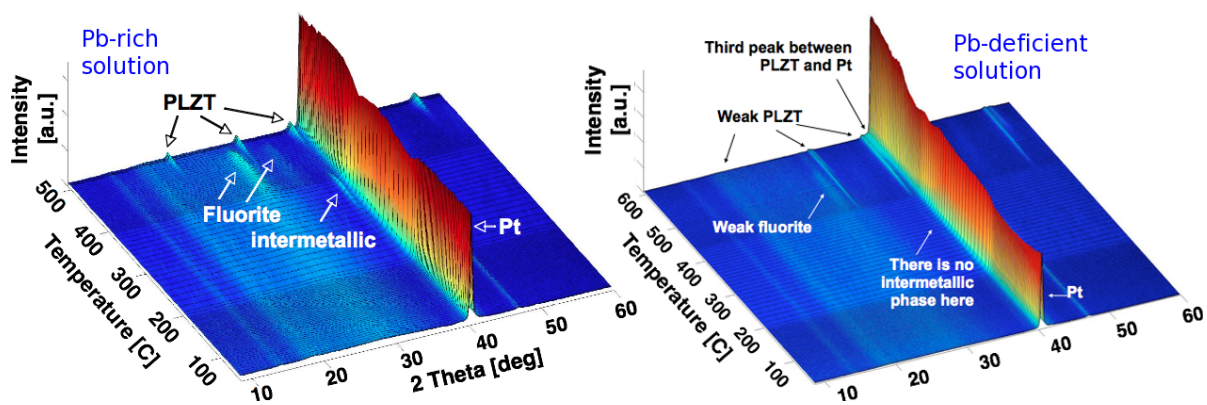

Figure 4.1. *in-situ* x-ray diffraction of PZT-based thin films established the sequence of phase formation during thermal processing and highlighted the role of Pb stoichiometry in the development of a transient interfacial intermetallic layer.

The ongoing diffraction work complements a chemical analysis tool that Chad Parish developed and adapted for this project. Because of the lower crystallization temperature of $PbTiO_3$ relative to $PbZrO_3$, solution-derived PZT thin films are often observed to be Ti-rich near the bottom electrode, a common source of heterogeneous nucleation sites, and Zr-rich near the films surface. Calame and Muralt showed that this effect can be counteracted by carefully tailoring the compositions of deposited layers, and used chemical depth profiles to support the claims of homogeneous B-site cation (Ti + Zr) distribution. [29] The Calame work is an excellent example of an engi-

neering solution to a difficult problem, but it also highlights a shortcoming of the analytical tools commonly available for use in such studies. Microstructural features in such films are commonly ∼100s of nm in size, while variations in cation distribution could (and has been seen to) occur on the order of individual nanometers. Surface-based techniques can achieve depth resolutions on the order of individual nanometers, but typically sample across 10s–100s of μm^2 of lateral area and therefore sample across many microstructural features (see Figure 4.2). At the other extreme are typical TEM EDS linescans which offer nanoscale resolution in the lateral dimension during a scan across the thickness of a film, but because of this are limited to looking at what is essentially a 1.5-dimensional slice out of a 3-dimensional sample. It is possible to string together a large number of EDS linescans in an attempt to increase the lateral expanse of the analysis, but the associated long acquisition times are not only inconvenient, but are complicated by unavoidable sample drift and, often, beam-induced sample damage.

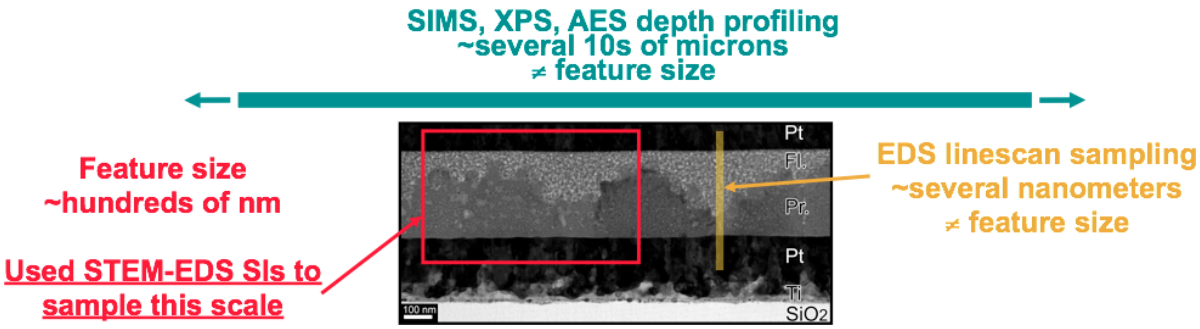

Figure 4.2. Spectral Imaging (SI) combines the high-resolution chemical information necessary to quantify cation distributions with the broad range required to connect measured variations to microstructural features.

Spectral imaging (SI) combined with advanced statistical analytical tools such as principle component analysis (PCA) and multi-variate statistical analysis (MVSA) enables the rapid collection of data at length scales relevant to both nm-level cation distributions as well as microstructural features, enabling researchers to associate measured distributions with microstructure, a critical capability that is not possible using other analytical techniques. What this means in a practical sense is that, with careful experimental setup and technique, we now have the capability of acquiring quantitative chemical maps across square microns of sample area with individual pixel resolution of ∼3–5nm. Not only has this tool verified the Pb deficiency of surface fluorite layers and confirmed the tendency of slowly-crystallized PZT films to be Ti-rich near the electrode and Zr-rich near the film surface, it also allowed us to discover the tendency for La and Zr to co-segregate during the crystallization of PLZT films (Figure 4.3). Significantly greater detail about the spectral imaging technique and its application to PZT-based thin film is available in the reference works. [30, 31, 32]

Structural and chemical analysis are indispensable tools for understanding the origins of ferroelectric and piezoelectric response, but in terms of material function and device performance, direct measurement of the desired electrical (and/or electromechanical) response is what really matters. Piezoelectric force microscopy (PFM) is a contact scanning probe technique where small distortions of the sample surface induced by an oscillating (ac) voltage applied with a conductive tip are

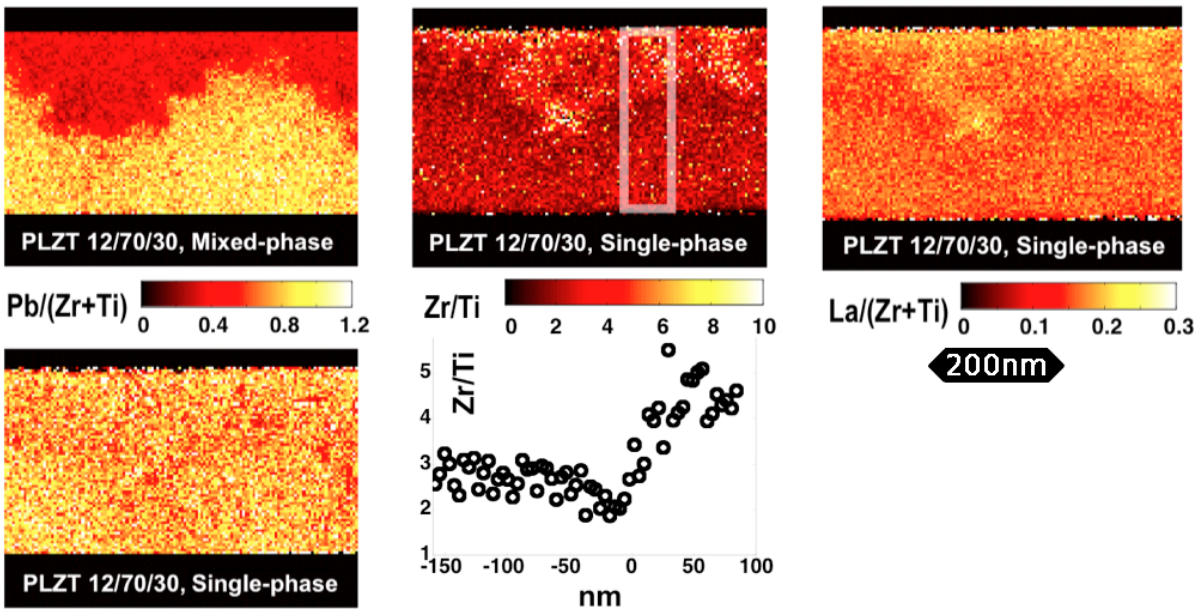

Figure 4.3. Chemical analysis enabled by the combination of SI, PCA, and MVSA can give quantitative chemical information on the ∼3-5nm level across micron-scale areas, providing a direct link between microstructural features and chemical distribution.

imaged. [33] This allows for the simultaneous acquisition of the topography and the amplitude and phase of the piezoelectric signal with respect to the applied voltage and is shown schematically in Figure 4.4.

While the PFM technique has been used extensively during the last decade to measure qualitative properties of piezoelectric and ferroelectric surfaces, it is still challenging to get quantitative measurements of the piezoelectric coefficients. Care must be taken in calibration to obtain quantitative results. To achieve high lateral resolution in measurements, a conductive AFM tip must be

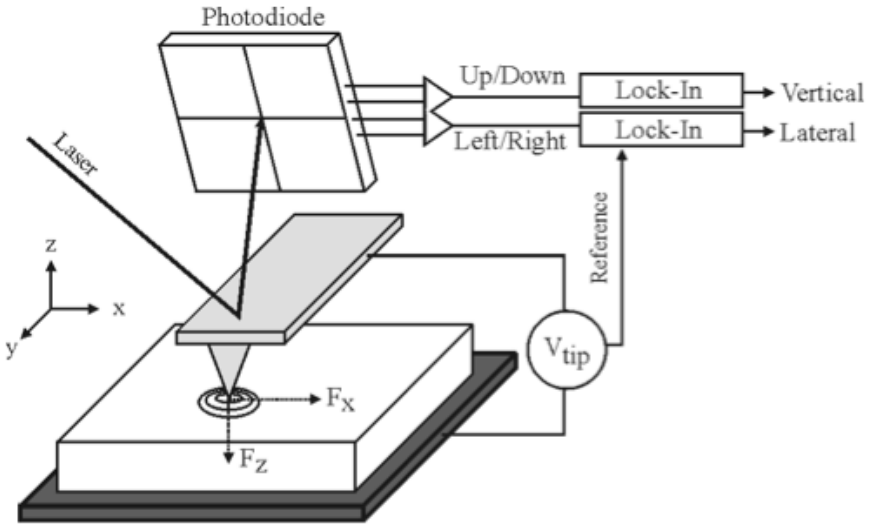

Figure 4.4. Schematic illustration of a PFM setup.

used as the top electrode. This produces an inhomogeneous and very localized electric field near the tip, which can induce local clamping and nonlinear surface responses [34] and leads to a non-trivial evaluation of the piezoelectric response. [35, 36] In measuring nanostructures, topographic artifacts can cause additional problems. [37] Despite these difficulties, this technique offers excellent resolution and is the most accessible experimental means to measure piezoelectric properties of nanomaterials.

For the current project, electromechanical response was measured for continuous and microscale patterned (using the MgO-mediated e-beam patterning approach described in Chapter 3) PZT films. AFM scans were also collected of amorphous nanopillars, but due to their amorphous nature, such features were not piezoelectric. The micro-patterned films exhibited a linear electromechanical response indicative of piezoelectricity; this response was also hysteretic, suggesting but not proving the existence of a reversible spontaneous polarization (*i.e.,* ferroelectricity) in these films. Figure 4.5 shows PFM data collected from one of these micropatterned PZT samples.

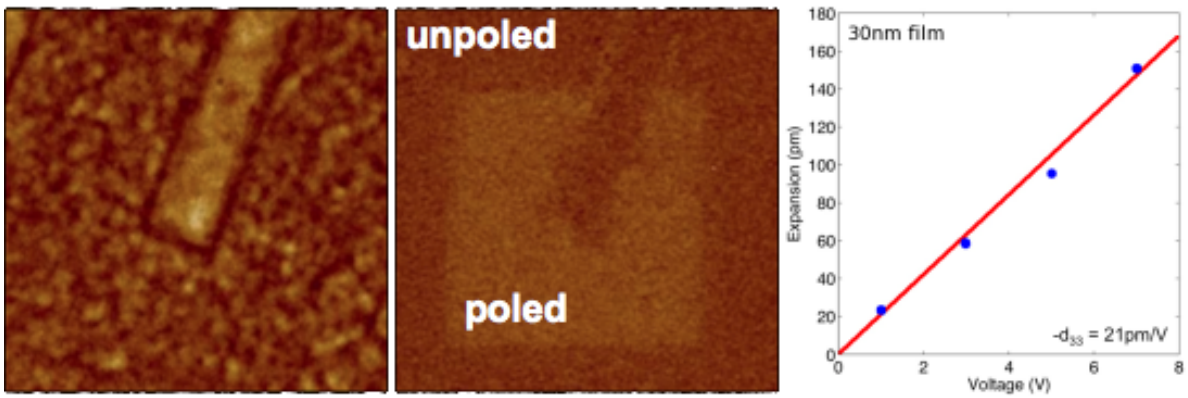

Figure 4.5. ∼30nm thick PZT thin films patterned using an MgO-mediated approach exhibited a piezoelectric response as measured by PFM. Scans shown in this figure are 10μm x 10μm.

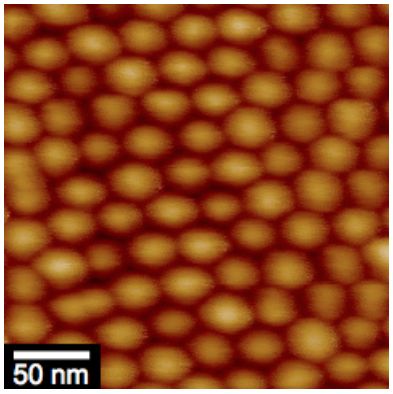

Figure 4.6. AFM scan of nanopatterned amorphous PZT features fabricated directly on Pt//Si using the BCP-liftoff technique.

Chapter 5

Conclusions

This project investigated patterning and integration techniques that would be compatible with PZT-based ultra-high density rad-hard NVRAM. In particular, the project focused on extending lithography techniques based on the directed self assembly of block copolymers to non-Si/SiO_2 substrate layers and studied techniques for integrating these discrete and ordered $\sim$20nm features into functional device structures. In addition to developing a fabrication platform that enables the formation of nanoscale feature of essentially any material that can be deposited by sputtering and/or chemical solution into ordered nanofeatures, this project also initiated in-depth *in-situ* diffraction studies of PZT-based thin films, laid the groundwork for etching and pattern transfer from and into a variety of non-standard materials at the extreme nanoscale, and developed characterization and analysis tools that can determine quantitative chemical distribution at the $\leq$5nm scale.

The project also helped SNL establish relationships with leading university professors (specifically Prof. John Ekerdt at the University of Texas at Austin, Profs. Paul Nealey and Padma Gopalan at the University of Wisconsin, and Prof. Jacob Jones at the University of Florida) which led to two follow-on projects with Profs. Nealey and Jones. The work in this project spanned basic to applied science and received significant recognition from outside of SNL, as evidenced by the 16 invited talks that resulted from these efforts. While substantial challenges remain for the integration of functional nanoscale ferroelectric features into working devices, the fabrication, integration, and analysis tools developed as part of this project have established the fundamental background essential to further development in this area.

References

[1] Y. C. Chen, C. T. Rettner, S. Raoux, G. W. Burr, S. H. Chen, R. M. Shelby, M. Salinga, W. P. Risk, T. D. Happ, G. M. McClelland, M. Breitwisch, A. Schrott, J. B. Philipp, M. H. Lee, R. Cheek, T. Nirschl, M. Lamorey, C. F. Chen, E. Joseph, S. Zaidi, B. Yee, H. L. Lung, R. Bergmann, and C. Lam. Ultra-thin phase-change bridge memory device using GeSb. *Electron Devices Meeting, 2006. IEDM '06. International*, pages 1–4, 2006.

[2] Semiconductor Industry Association. The international technology roadmap fo semiconductors: 2009 update, 2009.

[3] P. Muralt, Ronald G. Polcawich, and Susan Trolier-McKinstry. Piezoelectric thin films for sensors, actuators, and energy harvesting. *MRS Bulletin*, 34:658–664, 2009.

[4] W. Pan, C.L. Thio, and S.B. Desu. Reactive ion etching damage to the electrical properties of ferroelectric thin films. *Journal of Materials Research*, 13(2):362–367, February 1998.

[5] C. Soyer, E. Cattan, D. Remiens, and M. Guilloux-Viry. Ion beam etching of lead-zirconate-titanate thin films: Correlation between etching parameters and electrical properties evolution. *Journal of Applied Physics*, 92(2):1048–1055, July 2002.

[6] A. Stanishevsky, B. Nagaraj, J. MeIngailis, R. Ramesh, L. Khraichtchev, and E. McDaniel. Radiation damage and its recovery in focused ion beam fabricated ferroelectric capacitors. *Journal of Applied Physics*, 92(6):3275–3278, September 2002.

[7] Dillon D. Fong, G. Brian Stephenson, Stephen K. Streiffer, Jeffrey A. Eastman, Orlando Auciello, Paul H. Fuoss, and Carol Thompson. Ferroelectricity in ultrathin perovskite films. *Science*, 304(5677):1650–1653, 2004.

[8] D. A. Tenne, P. Turner, J. D. Schmidt, M. Biegalski, Y. L. Li, L. Q. Chen, A. Soukiassian, S. Trolier-McKinstry, D. G. Schlom, X. X. Xi, D. D. Fong, P. H. Fuoss, J. A. Eastman, G. B. Stephenson, C. Thompson, and S. K. Streiffer. Ferroelectricity in ultrathin $BaTiO_3$ films: Probing the size effect by ultraviolet raman spectroscopy. *Phys. Rev. Lett.*, 103(17):177601, Oct 2009.

[9] M.W. Matsen and M. Schick. Stable and unstable phases of a diblock copolymer melt. *Physical Review Letters*, 72(16):2660 – 2663, April 1994.

[10] M W Matsen. The standard Gaussian model for block copolymer melts. *Journal of Physics: Condensed Matter*, 14(2):R21, 2002.

[11] Frank S. Bates. Polymer-polymer phase behavior. *Science*, 251:898–905, February 1991.

[12] Marc A. Hillmyer, Frank S. Bates, Kristoffer Almdal, Kell Mortensen, Anthony J. Ryan, and J. Patrick A. Fairclough. Complex phase behavior in solvent-free nonionic surfactants. *Science*, 271(5251):976–978, 1996.

[13] Miri Park, Christopher Harrison, Paul M. Chaikin, Richard A. Register, and Douglas H. Adamson. Block copolymer lithography: Periodic arrays of $\sim 10^{11}$ holes in 1 square centimeter. *Science*, 276(5317):1401–1404, 1997.

[14] R. Olayo-Valles, M.S. Lund, C. Leighton, and M.A. Hillmyer. Large area nanolithographic templates by selective etching of chemically stained block copolymer thin films. *Journal of Materials Chemistry*, 14:2729–2731, 2004.

[15] Mark P. Stoykovich, Huiman Kang, Kostas Ch. Daoulas, Guoliang Liu, Chi-Chun Liu, Juan J. de Pablo, Marcus Müller, and Paul F. Nealey. Directed self-assembly of block copolymers for nanolithography: Fabrication of isolated features and essential integrated circuit geometries. *ACS Nano*, 1(3):168–175, 2007.

[16] Kosmas Galatsis, Kang L. Wang, Mihri Ozkan, Cengiz S. Ozkan, Yu Huang, Jane P. Chang, Harold G. Monbouquette, Yong Chen, Paul Nealey, and Youssry Botros. Patterning and templating for nanoelectronics. *Advanced Materials*, 22:769–778, 2010.

[17] Francois A. Detcheverry, Darin Q. Pike, Paul F. Nealey, Marcu Muller, and Juan J. de Pablo. Simulations of theoretically informed coarse grain models of polymeric systems. *Faraday Discussions*, 144:111–125, 2010.

[18] Shengxiang Ji, Guoliang Liu, Fan Zheng, Gordon S. W. Craig, F. J. Himpsel, and Paul F. Nealey. Preparation of neutral wetting brushes for block copolymer films from homopolymer blends. *Advanced Materials*, 20:3054–3060, 2008.

[19] Charles T. Black. Nanometer-scale pattern registration and alignment by directed diblock copolymer self-assembly. *IEEE Transactions on Nanotechnology*, 3(3):412–415, 2004.

[20] Rachel A. Segalman, Hideaki Yokoyama, and Edward J. Kramer. Graphoepitaxy of spherical domain block copolymer films. *Advanced Materials*, 13(5):1152–1155, 2001.

[21] Ion Bita, Joel K. W. Yang, Yeon Sik Jung, Caroline A. Ross, Edwin L. Thomas, and Karl K. Berggren. Graphoepitaxy of self-assembled block copolymers on two-dimensional periodic patterned templates. *Science*, 321:939–943, 2008.

[22] Ricardo Ruiz, Huiman Kang, Francois A. Detcheverry, Elizabeth Dobisz, Dan S. Kercher, Thomas R. Albrecht, Juan J. de Pablo, and Paul F. Nealey. Density multiplication and improved lithography by directed block copolymer assembly. *Science*, 321:936–939, 2008.

[23] Mark P. Stoykovich, Kostas Ch. Daoulas, Marcus Müller, Huiman Kang, Juan J. de Pablo, and Paul F. Nealey. Remediation of line edge roughness in chemical nanopatterns by the directed assembly of overlying block copolymer films. *Macromolecules*, 43:2334–2342, 2010.

[24] Eungnak Han, Insik In, Sang-Min Park, Young-Hye La, Yao Wang, Paul F. Nealey, and Padma Gopalan. Photopatternable imaging layers for controlling block copolymer microdomain orientation. *Advanced Materials*, 19:4448–4452, 2006.

[25] Geoff L. Brennecka, Chad M. Parish, Bruce A. Tuttle, and Luke N. Brewer. Multilayer thin and ultrathin film capacitors fabricated by chemical solution deposition. *Journal of Materials Research*, 23(1):176–181, 2008.

[26] B.A. Tuttle and R.W. Schwartz. Solution depostion of ferroelectric thin films. *MRS Bulletin*, 21(6):49–54, June 1996.

[27] Philip J. Kuekes, Gregory S. Snider, and R. Stanley Williams. Crossbar nanocomputers. *Scientific American*, pages 72–80, November 2005.

[28] Wei Lu and Charles M. Lieber. Nanoelectronics from the bottom up. *Nature Materials*, 6:841–850, November 2007.

[29] F. Calame and Paul Muralt. Growth and properties of gradient free sol-gel lead zirconate titanate thin films. *Applied Physics Letters*, 90:062907, 2007.

[30] Chad M. Parish, Geoff L. Brennecka, Bruce A. Tuttle, and Luke N. Brewer. Quantitative chemical analysis of fluorite-to-perovskite transformations in (Pb,La)(Zr,Ti)O_3 PLZT thin films. *Journal of Materials Research*, 23(11):2944–2953, November 2008.

[31] Chad M. Parish, Geoff L. Brennecka, Bruce A. Tuttle, and Luke N. Brewer. Quantitative x-ray spectrum imaging of lead lanthanum zirconate titanate PLZT thin-films. *Journal of the American Ceramic Society*, 91(11):3690–3697, 2008.

[32] Chad M. Parish and Luke N. Brewer. Multivariate statistics applications in phase analysis of STEM-EDS spectrum images. *Ultramicroscopy*, 110:134–143, 2009.

[33] Alexei Gruverman, Orlando Auciello, and Hiroshi Tokumoto. Imaging and control of domain structures in ferroelectric thin films via scanning force microscopy. *Annual Review of Materials Science*, 28:101–123, 1998.

[34] Tobias Jungk, Akos Hoffmann, and Elisabeth Soergel. Quantitative analysis of ferroelectric domain imaging with piezoresponse force microscopy. *Applied Physics Letters*, 89:163507, 2006.

[35] F. Felten, G.A. Schneider, J. Munoz Saldana, and S.V. Kalinin. Modeling and measurement of surface displacements in $BaTiO_3$ bulk material in piezoresponse force microscopy. *Journal of Applied Physics*, 96(1):563–568, July 2004.

[36] Sergei V. Kalinin, Eugene A. Eliseev, and Anna N. Morozovska. Materials contrast in piezoresponse force microscopy. *Applied Physics Letters*, 88:232904, 2006.

[37] F. Peter, A. Rudiger, and R. Waser. Mechanical crosstalk between vertical and lateral piezoresponse force microscopy. *Review of Scientific Instruments*, 77:036103, 2006.

DISTRIBUTION:

1	MS 1411	Geoff Brennecka, 1816
1	MS 1411	James Voigt, 1816
1	MS 1411	Bruce Tuttle, 1816
1	MS 0899	Technical Library, 9536 (electronic copy)
1	MS 0359	D. Chavez, LDRD Office, 1911

Sandia National Laboratories